Eur. Phys. J. A **25**, s01, 255–258 (2005)
DOI: 10.1140/epjad/i2005-06-110-5

EPJ A direct
electronic only

First experiment of ^{6}He with a polarized proton target

M. Hatano[1,2], H. Sakai[1,2,3,a], T. Wakui[3], T. Uesaka[3], N. Aoi[2], Y. Ichikawa[1], T. Ikeda[4], K. Itoh[4], H. Iwasaki[1], T. Kawabata[3], H. Kuboki[1], Y. Maeda[1], N. Matsui[5], T. Ohnishi[2], T.K. Onishi[1], T. Saito[1], N. Sakamoto[2], M. Sasano[1], Y. Satou[5], K. Sekiguchi[2], K. Suda[3], A. Tamii[6], Y. Yanagisawa[2], and K. Yako[1]

[1] Department of Physics, University of Tokyo, Hongo 7-3-1, Bunkyo, Tokyo 113-0033, Japan
[2] RIKEN, Hirosawa 2-1, Wako, Saitama 351-0198, Japan
[3] Center for Nuclear Study, University of Tokyo, Hirosawa 2-1, Saitama 351-0198, Japan
[4] Department of Physics, Saitama University, Shimo-Ohkubo 255, Saitama 338-8570, Japan
[5] Department of Physics, Tokyo Institute of Technology, Ohokayama 2-12-1, Meguro, Tokyo 152-0033, Japan
[6] Research Center for Nuclear Physics, Osaka University, Mihogaoka 10-1, Ibaraki, Osaka 567-0047, Japan

Received: 15 November 2004 /
Published online: 30 June 2005 –

Abstract. We have constructed a new type of spin polarized solid proton target which can be operated under a low magnetic field of 0.08 T and a high temperature of 100 K. We have measured for the first time the polarization asymmetry of an unstable beam of ^{6}He at an energy of 71 MeV/u. Optical potential analyses have been carried out.

PACS. 24.70.+s Polarization phenomena in reactions – 25.40.Cm Elastic proton scattering – 27.20.+n $6 \leq A \leq 19$

1 Introduction

Radio-isotope (RI) beam experiments have extended the horizon of research to nuclei far from the stability line. Nuclear reactions with a spin polarized beam have been continuously giving us precious information both on nuclear structure and on reaction mechanisms. In order to apply such polarization measurements to the RI beam experiments, a polarized proton target is necessary. The first choice would be a polarized gas proton target type since it has been established technically. However a low density of the gas target coupled with a low intensity of RI beam, *i.e.* low luminosity, makes the RI beam experiment very difficult. Inevitably the second choice would be a polarized solid proton target (PSPT) system. A conventional PSPT system which requires a high magnetic field (≥ 2.5 T) and a very low temperature (≤ 1 K) is inconvenient for the RI beam experiments. This is because the RI beam experiments utilize inverse kinematics. Therefore it involves detection of low energy protons or deuterons which are emitted to large angles ($> 50^\circ$ in the lab. system). The detection of such low energy particles is very difficult under such severe environment. We have constructed a PSPT which overcomes those drawbacks and allows us to pursue various spin polarized experiments with RI beams.

[a] Conference presenter;
e-mail: sakai@phys.s.u-tokyo.ac.jp

2 Construction OF PSPT

Our target material is a crystal of naphthalene (host) doped with pentacene (guest). It was first reported by Henstra that a proton in this aromatic material can be polarized under a low magnetic field and at a high temperature [1].

The basic principle to polarize a proton is a pulsed dynamic nuclear polarization (DNP) method. First, an alignment of electron population which appears in the lowest triplet state of pentacene is produced by means of optical pumping by a laser. Maximum magnetic substate populations are $|m = 0\rangle = 76\%$ and $|m = \pm 1\rangle = 12\%$. This electron alignment is subsequently transferred to a proton polarization by using the integrated solid effect (ISE). The maximum proton polarization is expected to be 72.8%, if the polarization transfer is perfect and relaxation of polarization is negligible.

We first constructed a PSPT system for the off-line test which consisted of a C-type magnet, the laser system with an Ar-ion laser operated at 514 nm and the cylindrical cavity with a microwave generator with 9.1 GHz. By using this system we have achieved a proton polarization of about 37% under the magnetic field of 0.3 T and the temperature of 100 K with a naphthalene crystal size of $4 \times 5 \times 2\,\mathrm{mm}^3$ [2]. The relaxation time was measured to be about 22 hours.

Based on this experience gained in off-line tests we designed a PSPT system which could operate under the experimental conditions required by the RI beam [2,3]. Firstly, we needed to produce a large and thin target crystal made of naphthalene doped with pentacene to cope with a large size of the RI beam due to the secondary beam. Secondly, a completely new design was needed for the resonator system of microwave, to keep minimum material along the recoil proton trajectory to avoid energy loss. We introduced a loop-gap resonator which is made of a Teflon thin film of 25 μm on both sides of which copper stripes with a thickness of 4.4 μm are printed [4]. Finally, special care was taken for the target chamber design to cool down the target. The target chamber has another small chamber nesting inside it. The small chamber in which the target crystal and the devices for polarizing the target such as the loop-gap resonator are equipped is cooled by cold nitrogen gas. The volume between the two chambers is evacuated and connected to the beam pipe. Each chamber has a glass window for the laser light input and three exit windows with thin Kapton foils (50 μm), one for the beam and two for the recoil particles at left and right sides of the chambers with respect to the beam direction.

3 Polarization measurement

The first polarization asymmetry measurement [3] was performed with the unstable beam of ^{6}He with 71 MeV/u produced by the RIKEN Projectile-fragment Separator (RIPS). We chose elastic scattering since the event identification is relatively easy. Moreover, the cross-section data existed for the scattering angle of $\theta_{\rm cm} = 20°$–$50°$ [5]. The cross-section and the polarization asymmetry (= target polarization × analyzing power) were measured for $\theta_{\rm cm} = 40°$–$80°$ which covers the second diffraction peak of cross-sections. This angle region is very interesting since all optical model predictions based on a microscopic folding model [6,7] or a phenomenological model [8] show a large *positive* polarization asymmetry, *i.e.* positive analyzing powers. The PSPT system was operated under a magnetic field of 0.08 T and a temperature of 100 K. The target crystal had a thickness of 1 mm with a diameter of 14 mm. The spot size of the ^{6}He beam was about 10 mm in diameter (FWHM) and its intensity was on the average 1.7×10^5 particles/s. The proton polarization during the measurement was monitored by a pulsed NMR method. The NMR amplitude as a function of time is shown in fig. 1. The direction of the polarization was reversed during the experiment to minimize the systematic uncertainties associated with geometry.

The scattered ^{6}He were detected by a multi-wire drift counter (MWDC) and three planes of plastic scintillator hodoscopes. The recoil protons were detected by the multi-stripped position sensitive silicon detectors backed by the plastic scintillation counters on left and right sides with respect to the beam.

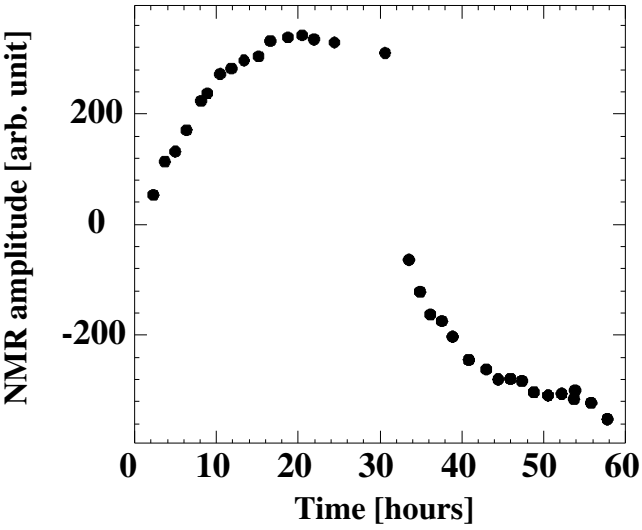

Fig. 1. NMR amplitudes during the measurement.

The polarization asymmetry ϵ can be derived from the measurement by

$$\epsilon = \frac{\sqrt{Y} - 1}{\sqrt{Y} + 1}\,, \tag{1}$$

$$Y = \frac{N_L^{\uparrow} \cdot N_R^{\downarrow}}{N_L^{\downarrow} \cdot N_R^{\uparrow}}\,, \tag{2}$$

where $N_{L(R)}^{\uparrow(\downarrow)}$ is the count detected by the left(right) $L(R)$ detector with the target polarization state "up"("down") $\uparrow$ ($\downarrow$).

ϵ is related to the target polarization P_t and the analyzing power A_y for the elastic scattering as

$$\epsilon = P_t \times A_y\,. \tag{3}$$

To derive A_y we need to know P_t. Unfortunately, we could not perform the calibration of P_t during the experiment and we thus made our best guess on the P_t value. We assumed $P_t = 0.21$. Systematic uncertainty of P_t could be as large as 50%. Note that this brings a large ambiguity in the magnitude of A_y but never changes its sign.

Figure 2 shows the cross-sections and the analyzing powers for the $\boldsymbol{p} + ^6$He scattering at 71 MeV/u as a function of c.m. scattering angles. Present results are plotted by solid circles and previous results by Korsheninnikov [5] are plotted by open circles. Only statistical errors are shown in this figure. Errors for the cross-section are smaller than the size of the symbol in most cases. Systematic error for the cross-section is estimated to be ±9%. For the analyzing powers, the horizontal bar indicates the bin width of the angle integrated.

It might be very interesting to compare our $\boldsymbol{p}+^6$He results to those of $\boldsymbol{p} + ^6$Li at the similar bombarding energy by Henneck [9]. The $\boldsymbol{p} + ^6$Li data are plotted by the open square symbols in fig. 2. It is surprising to find that the magnitude and the angular dependence of cross-sections are almost identical. This indicates that both nuclei have a

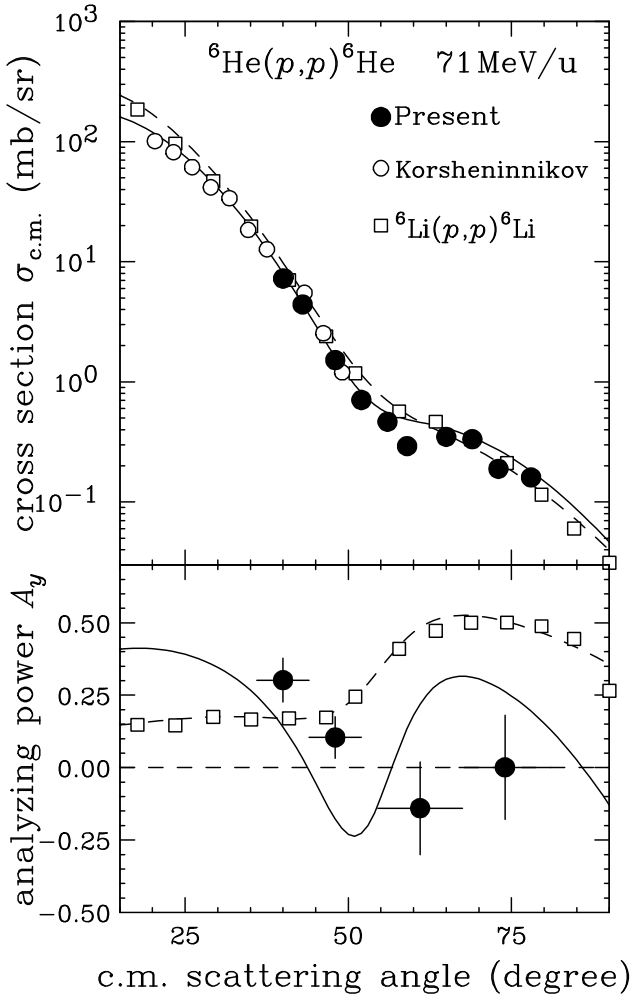

Fig. 2. Cross-sections and analyzing powers. See text for detail.

similar potential strength, *i.e.* radius and depth. However, it is even more surprising to find that the observed polarization asymmetry shows a remarkable difference between the $\boldsymbol{p}$+^{6}He and $\boldsymbol{p}$+^{6}Li scatterings. The polarization asymmetry changes the sign from positive to negative values for $\boldsymbol{p}+{}^6$He, while it increases rapidly from the small positive value to the large positive value for the same angular range in case of $\boldsymbol{p}+{}^6$Li. This feature of the *negative* values contradicts largely with the optical model predictions [6,7,8].

4 Analysis and discussion

We have carried out the optical model analysis by using the cross-section data. The standard Wood-Saxon shape is assumed for real and imaginary central potentials (V_R and W_R). The cross-sections are easily reproduced by the calculation as shown in the upper panel of fig. 2.

Obtained parameters are shown in table 1. For a comparison purpose, those by Henneck [9] for the $\boldsymbol{p}+{}^6$Li reaction at 72 MeV/u are included in table 1 and plotted in fig. 2 with the dashed curve.

Table 1. Optical potential parameters for $p+{}^6$He and $p+{}^6$Li reactions at 71 MeV/u and 72 MeV/u. V_i is in unit of MeV and r_i and a_i are in unit of fm. See text for detail.

Nucleus	V_R	r_R	a_R	W_v	r_{wv}	a_{wv}
^{6}He	−20.2	1.27	0.57	−19.2	0.92	0.64
^{6}Li	−31.7	1.10	0.75	−14.1	1.15	0.56
	$V_{\ell s}$	$r_{\ell s}$	$a_{\ell s}$			
^{6}He	−3.36	1.30	0.94			
^{6}Li	−3.36	0.90	0.94			

Table 2. Root mean square radius.

Nucleus	$\langle r^2\rangle^{\frac{1}{2}}_{\rm pot}$(fm)
^{6}He	2.76(10)
^{6}Li	3.18(28)

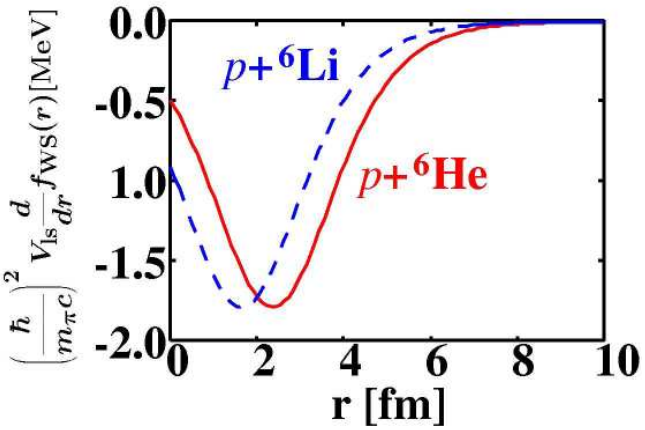

Fig. 3. Shape of the spin-orbit potential. See text for detail.

From the real central part of the optical potential, the mean square radius of the potential $\langle r^2\rangle_{\rm pot}$ can be evaluated by

$$\langle r^2\rangle_{\rm pot} = \int r^2 V_R(\mathbf{r})\mathrm{d}^3\mathbf{r} \Big/ \int V_R(\mathbf{r})\mathrm{d}^3\mathbf{r}. \qquad (4)$$

The root mean square radii for ^{6}He and ^{6}Li are shown in table 2. The root mean square radius of ^{6}Li is slightly larger than that of ^{6}He. This could be due to a d-α cluster structure of ^{6}Li.

It should be noted that the mean square radius is related with the mean square matter distribution $\langle r^2\rangle_{\rm matt}$ and the mean square interaction radius $\langle r^2\rangle_{\rm int}$ as

$$\langle r^2\rangle_{\rm pot} = \langle r^2\rangle_{\rm matt} + \langle r^2\rangle_{\rm int}\,, \qquad (5)$$

for a nucleus with a rotationally symmetric density distribution. A Glauber based analysis of the experimental elastic scattering of the $p+{}^6$He scattering at 0.7 GeV gives $\langle r^2\rangle^{\frac{1}{2}}_{\rm matt} \simeq 2.3-2.4$ fm [10] which is smaller than

the present result by the mean square interaction radius of $\langle r^2 \rangle_{\rm int}^{\frac{1}{2}} \simeq 1.5\,{\rm fm}$.

Since the polarization asymmetry data are poor in statistics and only 4 angles exist, it is difficult to make an automatic parameter search for the spin-orbit potential $V_{\ell s}$. Here the Thomas type is used for $V_{\ell s}$. Thus we changed parameters ($V_{\ell s}$, $r_{\ell s}$, $a_{\ell s}$) by hand and tried to get a better fit by eyes! The peculiar behavior of the sign change of A_y can be better reproduced when $r_{\ell s}$ is set to be larger compared to the standard value in this mass region. One example of such fit is shown in the lower panel of fig. 3 by the solid curve.

In fig. 3 the shapes of the spin-orbit potential are shown for ^{6}He (solid curve) and ^{6}Li (dashed curve), respectively. The spin-orbit potential for ^{6}He seems to locate outside further by about 0.8 fm compared to that for ^{6}Li.

It is interesting to note that the angular behavior of the present polarization asymmetry of $\boldsymbol{p} + {}^6$He at 71 MeV/u is very similar to that of $\boldsymbol{p} + {}^4$He at 72 MeV/u [11].

5 Summary

A polarized solid proton target which works under the condition of a low magnetic field of 0.8 T and a high temperature of 100 K has been built and used, for the first time, for the polarization asymmetry measurement with the ^{6}He beam at 71 MeV/u. The asymmetry shows an unexpected behavior which disagrees with the optical model predictions.

The present work has demonstrated the usefulness of the polarization measurement for exploring a new aspect of unstable nuclei.

We would like to thank I. Tanihata and T. Suda for their continuous support on this work. We are indebted to M. Iinuma and K. Takeda for helpful suggestions in the early stage of this work. We also wish to thank the RIKEN accelerator group for their excellent work. This work has been supported in part by the Grant-in-Aid for Scientific Research No. 15740139 of the Ministry of Education, Culture, Sports, Science, and Technology of Japan.

References

1. A. Henstra, T.-S. Lin, J. Schmidt, W.Th. Wenckebach, Chem. Phys. Lett. **165**, 6 (1990).
2. T. Wakui, M. Hatano, H. Sakai, A. Tamii, T. Uesaka, AIP Conf. Proc. **675**, 911 (2003); T. Wakui *et al.*, Nucl. Instrum. Methods A **526**, 182 (2004).
3. M. Hatano, PhD Thesis, University of Tokyo, unpublished (2004).
4. T. Uesaka *et al.*, Nucl. Instrum. Methods A **526**, 186 (2004).
5. A.A. Korsheninnikov *et al.*, Nucl. Phys. A **616**, 45 (1997).
6. S.P. Weppner, O. Garcia, Ch. Elster, Phys. Rev. C **61**, 044601 (2000).
7. K. Amos, private communication.
8. D. Gupta, C. Samanta, R. Kanungo, Nucl. Phys. A **674**, 77 (2000).
9. R. Henneck *et al.*, Nucl. Phys. A **571**, 541 (1994).
10. G.D. Alkhazov *et al.*, Nucl. Phys. A **712**, 269 (2002).
11. J. Campbell *et al.*, Phys. Rev. C **39**, 56 (1989).